Available online at www.sciencedirect.com

ScienceDirect

IFAC PapersOnline CONFERENCE PAPER ARCHIVE

IFAC PapersOnLine 59-37 (2025) 280–285

Enhanced Control Technique for Dual-Star Induction Machine Drive: A Fractional-Order Controller-Based DTC Approach with Virtual Voltages

Guedida Sifelislam * **Tabbache Bekheira** * **Nounou Kamal** * **Nesri Mokhtar** ** **Benzaoui Khaled Mohammed Said** *** **Idir Abdelhakim** ****

* *UER ELT, Ecole Militaire Polytechnique, Algiers, Algeria (e-mail: guedida.sifelislam@gmail.com, bekheira.tabbache@emp.mdn.dz, kamel.nounou@emp.mdn.dz).*

** *École Supérieure Ali Chabati, Reghaia, Alger, Algérie (e-mail: nesri_m@yahoo.fr)*

*** *Faculté des Sciences Appliquées, Laboratoire LAGE, Université de Ouargla, Ouargla, Algérie, (e-mail: benzaoui.khaled@univ-ouargla.dz)*

**** *Department of Electrical Engineering, University Mohamed Boudiaf of M'sila, M'sila, Algeria, (e-mail: abdelhakim.idir@univ-msila.dz)*

Abstract: Fractional calculus is the most popular form of control engineering in many fields, including electric drive applications. One of the most common applications in all fields of electric drives is the control of the dual-star induction machine (DSIM). Several control techniques have been proposed for this type of multiphase motor, ranging from classical PID-based methods to the most sophisticated advanced methods, including fractional-order controllers. Furthermore, in the case of a DSIM, which has been widely studied recently, inevitable harmonic currents are generated, which is a major problem and leads to increased losses and reduced system efficiency. Therefore, this paper presents a fractional order controller optimized using a dedicated method to improve system performance while minimizing overshoot, reducing response time, and minimizing rejection time, and a modified switching table has been developed to reduce harmonic currents using virtual voltage vectors. Simulation results validate the effectiveness of the proposed method.

Keywords: Direct torque control (DTC), Dual star induction motor (DSIM), harmonic currents, fractional order proportional-integral (FOPI), oustaloup approximation.

1. INTRODUCTION

Multiphase drive systems have been researched extensively for nearly five decades due to their superior characteristics compared to traditional 3-phase drive systems. The inherent redundancy of phase in these drives offers additional benefits, such as free-phase detection and improved fault-tolerant behavior Levi (2008); Duran et al. (2017). DSIM drives are considered an attractive topology among polyphase drives due to their robust mechanical design and flexible three-phase structure.

The Direct Torque Control (DTC) strategy is among the most extensively researched methods for managing multiphase electric drive systems. It operates by employing a switching table to choose suitable voltage vectors that regulate both the electromagnetic torque and the stator flux. The DTC has the advantages of a simple structure, rapid torque response, and independence from machine parameters. However, since large voltage vectors are in use, the machine is inevitably associated with significant harmonic currents. Hence, reducing these harmonic currents is essential to enhance the overall efficiency of the system Guedida et al. (2023); Boukhalfa et al. (2022).

Moreover, enhancing the dynamic performance of DTC in multiphase drive systems is crucial, and numerous studies have been conducted to achieve superior response characteristics Guedida et al. (2024); Terfia et al. (2023). Moreover, it is important to emphasize that the conventional speed control loop commonly employs a Proportional–Integral (PI) controller, whose performance relies on the accuracy of the system's mathematical model. For this reason, a recent study proposes a technique for tuning the PI controller of the DSIM speed loop, based on DTC control, using genetic algorithms and neuro-fuzzy schemes to improve machine performance Belal et al. (2024). However, determining the appropriate parameters of the conventional PI controller is challenging when dealing with external disturbances or variations in machine parameters, making it difficult to achieve fast response, minimal

10.1016/j.ifacol.2026.01.048

overshoot, and high precision in terms of both speed and electromagnetic torque.

Fractional-order proportional-integral (FOPI) controllers have recently attracted considerable academic and industrial interest Idir et al. (2025). This controller represents an extended version of the classical PI controller, which was first proposed by Podlubny Podlubny et al. (1999) in 1997. Several studies have indicated that implementing FOPI controllers yields superior performance compared to approaches utilizing the classical PI controller Chagam and Devabhaktuni (2022). Furthermore, according to the study conducted by Gude et al. (2023), they demonstrated good performance, noise rejection, and robustness when comparing the performance of the classical PI controller and the fractional-order PI controller, which were tuned using a particle swarm optimization (PSO) and differential evolution optimization algorithm for speed control of a DC motor.

This paper presents a modified DTC for the DSIM, based on the use of virtual voltage vectors and a FOPI controller. The aim of employing virtual voltage vectors is to minimize harmonic currents and to generate purely sinusoidal phase currents. Furthermore, this work also uses the advantages of a FOPI controller with a PSO optimization algorithm in the speed controller loop to improve speed and torque response in the machine. The dynamic performance of the proposed technique is tested by simulation results. These results demonstrate a substantial reduction in harmonic currents and a notable improvement in the transient responses of both electromagnetic speed and torque.

2. MATHEMATICAL MODEL OF THE DSIM

Figure 1 shows the DSIM drive system powered by a six-leg inverter. By applying the vector decomposition method (VSD), the 6-dimensional electromechanical model can be separated into three decoupled subspaces. Zhao, Y., and Lipo, T. A. (1995).

The harmonic components of order l=12r±1 are mapped onto the $(\alpha - \beta)$, whereas those of order l=6r±1 are projected onto the $(x - y)$. The components of zero-sequence, corresponding to harmonics of order l=3r , are represented in the $(o1 - o2)$ subspace. However, the components in $(o1 - o2)$ when the neutral points are separated, as shown in Figure 1(b).

The DSIM model obtained can be formulated as follows Guedida et al. (2023):

$$V_{s\alpha\beta} = R_s I_{s\alpha\beta} + \frac{d\psi_{s\alpha\beta}}{dt} \quad (1)$$

$$\psi_{s\alpha\beta} = L_{s\alpha\beta} I_{s\alpha\beta} + \psi r\alpha\beta. \quad (2)$$

$$V_{sxy} = R_s I_{sxy} + \frac{d\psi_{sxy}}{dt} \quad (3)$$

$$\psi_{sxy} = L_{ls} I_{sxy} \quad (4)$$

$$V_{so1o2} = R_s I_{so1o2} + \frac{d\psi_{so1o2}}{dt} \quad (5)$$

$$\psi_{so1o2} = L_{ls} I_{so1o2} \quad (6)$$

$$V_{r\alpha\beta} = 0 = R_r I_{r\alpha\beta} + \frac{d\psi_{r\alpha\beta}}{dt} \pm \omega_r \psi_{r\alpha\beta} \quad (7)$$

$$\psi_{r\alpha\beta} = L_{r\alpha\beta} I_{r\alpha\beta} + \psi s\alpha\beta. \quad (8)$$

$$T_e = p(\psi_{s\alpha} * I_{s\beta} - \psi_{s\beta} * I_{s\alpha}) \quad (9)$$

Where:

$V_{s\alpha\beta}, V_{sxy}, V_{so1o2}$: are the stator voltages.

$I_{s\alpha\beta}, I_{sxy}, I_{so1o2}$: are the stator currents.

$\psi_{s\alpha\beta}, \psi_{sxy}, \psi_{so1o2}$: are the stator flux.

$V_{r\alpha\beta}$: is the rotor voltage.

$I_{r\alpha\beta}$: is the rotor current.

L_m, L_{ls}, $L_{r\alpha\beta} = L_{ls} + \frac{3}{2}L_m$ and $L_{s\alpha\beta} = L_{ls} + 3L_m$ are the magnetizing inductance and the leakage inductance of the rotor and stator.

R_s, R_r, p and T_e are the stator and rotor resistance, the number of pole pairs, and the electromagnetic torque, respectively.

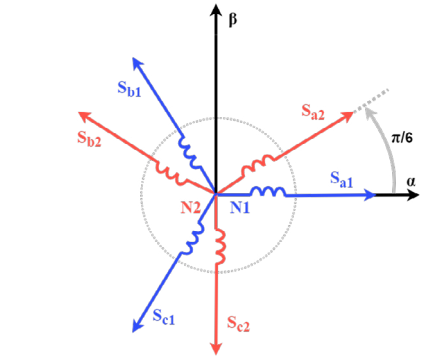

(a) DSIM machine

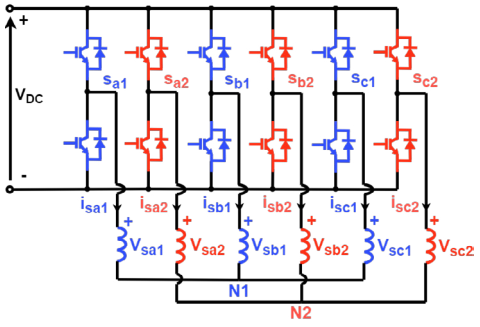

(b) DSIM fed by voltage source inverter

Fig. 1. Dual star induction motor and VSI-fed drive

As indicated in (9), the electromagnetic torque produced by the machine is influenced solely by the components of the subspace $(\alpha - \beta)$. Conversely, (3) and (4) show that the subspace $(x-y)$ components are the main contributors to the significant harmonic currents resulting from low impedance.

Figure 1 illustrates the DSIM supplied by a six-leg inverter. By using the binary representation of the voltage vectors $(S_{a1}S_{b1}S_{c1}S_{a2}S_{b2}S_{c2})$, it is possible to generate 64 switching combinations. As illustrated in Figure 3, it is clear that the 60 non-zero voltage vectors are distributed among four distinct dodecagons, designated as D_1, D_2, D_3, and D_4. The voltage vector amplitudes for each dodecagon in $(\alpha-\beta)$ are provided as follows Guedida et al. (2023, 2025); Ren et al. (2014):

$$V_{D4} = \frac{2}{3} V_{dc} cos(15)^0 = \frac{\sqrt{6}+\sqrt{2}}{6} V_{dc} \quad (10)$$

$$V_{D3} = \frac{2}{3} V_{dc} cos(45)^0 = \frac{\sqrt{2}}{3} V_{dc} \quad (11)$$

$$V_{D2} = \frac{1}{3} V_{dc} \quad (12)$$

$$V_{D1} = \frac{2}{3} V_{dc} cos(75)^0 = \frac{\sqrt{6}-\sqrt{2}}{6} V_{dc} \quad (13)$$

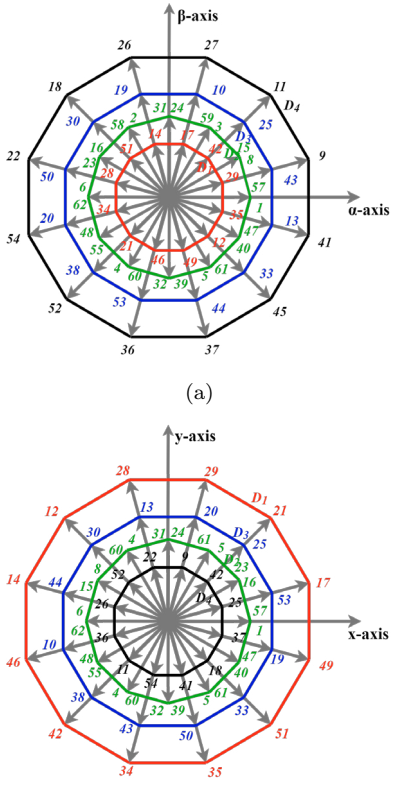

(a)

(b)

Fig. 2. Voltage vectors of the inverter in two subspaces: (a) α-β subspace, (b) x-y subspace

3. BASICS FRACTIONAL CALCULUS

Fractional calculus is a field of mathematics that extends traditional concepts of integration and differentiation to include non-integer orders. When the order n takes values of irrational-fractional complex, FC provides a framework for computing n-fold integrals or derivatives, such as $d^n y/dt^n$. In recent years, there has been a significant increase in fractional calculus (FC) applications. The mathematical properties of these approaches make it possible to achieve a high level of accuracy in characterizing a real object compared with conventional methods based on integer-order mathematics. The following notation represents the generalized fundamental operator:

$$aD_t^{\alpha} = \begin{cases} \dfrac{d^{\alpha}}{dt^{\alpha}} & , R(\alpha) > 0 \\ 1 & , R(\alpha) = 0 \\ \displaystyle\int_a^t (d\tau)^{-\alpha} & , R(\alpha) < 0 \end{cases} \quad (14)$$

Where:

a represents the lower limit of integration.
t represents the upper limit of integration.

It is important to note that $\alpha \in R$, Sabatier et al. (2003).

The definition of the Grunwald–Letnikov (GL) fractional derivative is presented as follows:

$$aD_t^{\alpha} f(t) = \lim_{h \to 0} \frac{1}{h^{\alpha}} \sum_{r=0}^{\frac{(t-a)}{h}} (-1)^r \binom{\alpha}{r} f(t - rh) \quad (15)$$

Where $\omega_r^{(\alpha)} = (-1)^r \binom{\alpha}{r}$ is the polynomial coefficients of $(1-z)^{\alpha}$

Furthermore, the coefficients can be obtained recursively from:

$$\omega_0^{\alpha} = 1,\ \omega_r^{\alpha} = (1 - \frac{\alpha+1}{r})\, \omega_{r-1}^{\alpha},\ r = 1, 2, 3, \ldots \quad (16)$$

The Riemann–Liouville (RL) definition is expressed as follows:

$$aD_t^{-\alpha} f(t) = \frac{1}{\Gamma(\alpha)} \int_a^t (t-\tau)^{\alpha-1} f(\tau) d\tau \quad (17)$$

With $0 < \alpha < 1$, h is step time, and α generally taken to be zero, indicates the first occurrence. Hereafter, differentiation is expressed as $D_t^{-\alpha} f(t)$.

The Caputo definition is given as follows:

$$0D_t^{-\alpha} y(t) = \frac{1}{\Gamma(1-\gamma)} \int_a^t \frac{y^{m+1}(\tau)^{\alpha-1}}{(t-\tau)\gamma} d\tau \quad (18)$$

The Riemann–Liouville and Grunwald–Letnikov formulations have been shown to be equivalent for many functions encountered in real physical systems and a wide range of industrial applications Garrappa, R. (2014).

4. IMPROVEMENT OF THE DTC SCHEME FOR THE DSIM

4.1 DTC Based on Virtual Voltage Vectors

In order to minimize harmonic currents in the (x-y) subspace, a modification to the switching table of the DTC is necessary. The idea is based on replacing the 12 traditional voltage vectors with 12 virtual voltage vectors.

Figure 2 illustrates that the voltage vectors located in dodecagons D_1, D_3, and D_4 share the same direction in the $(\alpha - \beta)$ subspace, whereas the vectors of D_1 and D_4 have an opposite direction to that of D_3 in the $(x-y)$ subspace. The objective is to generate a new voltage vector whose amplitude is close to that of D_4 in the $(\alpha - \beta)$ subspace and zero in the $(x - y)$ subspace.

According to (19) and (20), and Fig. 3(b), the magnitude of the tension vectors of dodecagons D_3 and D_4 in (x-y) can be defined as follows:

$$V_{D4-xy} = \frac{\sqrt{6}-\sqrt{2}}{6} V_{dc} \quad (19)$$

$$V_{D3-xy} = \frac{\sqrt{2}}{3} V_{dc} \quad (20)$$

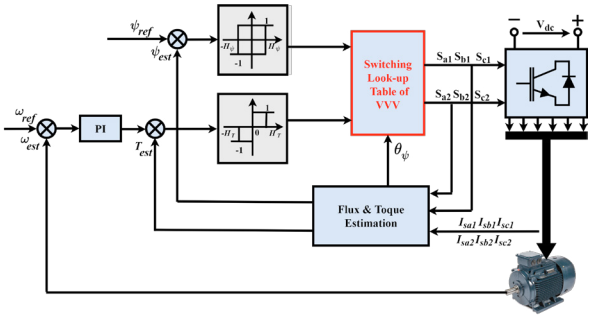

Fig. 3. Block diagram of the modified DTC based on virtual voltage vector

Therefore, to minimize the stator flux magnitude in the $(x-y)$ subspace, the durations T_{D3} and T_{D4} of the corresponding voltage vectors within one sampling period are defined as follows:

$$\frac{\sqrt{6}-\sqrt{2}}{6}V_{dc}T_{D4} = \frac{\sqrt{2}}{3}V_{dc}T_{D3} \tag{21}$$

$$T_{D4} + T_{D3} = T_s \tag{22}$$

From (21) and (24), it is possible to calculate the action times of the tension vectors of dodecagons D_3 and D_4 as follows:

$$T_{D4} = (\sqrt{3}-1)T_s \tag{23}$$

$$T_{D3} = (2-\sqrt{3})T_s \tag{24}$$

Therefore, by using the voltage vectors of the two dodecagons D_3 and D_4 with their new action times for one sampling period, it is possible to reduce harmonic currents in subspace $(x-y)$ effectively.

Table 1. Switching table for DTC

Sector k	$\varepsilon_T = 1$	$\varepsilon_T = -1$	$\varepsilon_T = 0$
$\varepsilon_\psi = 1$	V_{k+2}	V_{k-3}	V_{zero}
$\varepsilon_\psi = -1$	V_{k+3}	V_{k-4}	V_{zero}

The functional block diagram of the DTC system utilizing a switching-table with virtual voltage vectors is illustrated in Figure 3. The appropriate voltage vector is selected based on the torque control, the stator flux control, and the stator flux position, as defined in Table 1. The flux and torque control are generated through controllers, respectively. When these virtual voltage vectors are applied in the $(\alpha-\beta)$ subspace, their corresponding amplitudes in the $(x-y)$ subspace effectively reduce harmonic current components.

4.2 DTC-FOPI Speed Controller Design

Conventional PI controllers are extensively applied across various domains because of their straightforward implementation and simple structural design. The dynamic response of electromagnetic speed and torque in DTC for multiphase drives can be enhanced by the use of a FOPI controller. The basic principle of the classic PI controller consists of applying two actions, proportional and integral, to control the error signal. The transfer function of the classic PI controller is given by:

$$G_{PI}(s) = K_p + \frac{K_i}{s} \tag{25}$$

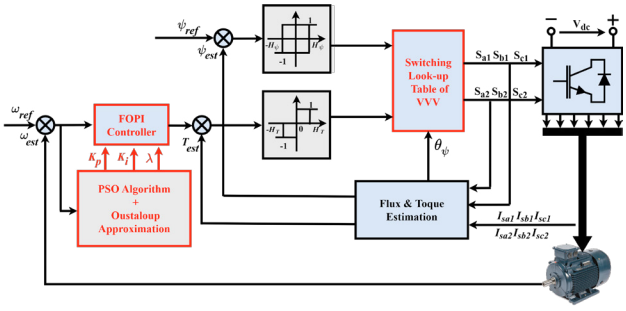

Fig. 4. Block diagram of the proposed DTC

Where:
K_p: is proportional gain.
K_s: is integral gain.

The FOPI controller shown in (26) is an enhanced extension of the classical PI controller, incorporating a λ-order integration that can take any positive real value.

$$G_{FOPI}(s) = K_p + \frac{K_i}{s^\lambda} \tag{26}$$

Where:
λ: is fractional order integration.

In order to compensate for the error between the desired speed and the measured value, a proposed approach is based on the FOPI controller using a PSO optimization algorithm in modified DTC for DSIM. Figure 4 shows the speed controller loop with the PSO/FOPI controller using the Oustaloup approximation Oustaloup et al. (2000). The purpose of employing these filters is to approximate the fractional-order transfer function with an equivalent integer-order representation.

5. SIMULATION RESULTS

In this section, simulation results have been obtained using MATLAB/SIMULINK software to demonstrate the benefits of using a FOPI controller based on the PSO optimization algorithm in the modified DTC control of the DSIM. The machine-specific parameters are identified and provided in Nesri et al. (2020).

The parameters of the FOPI controller are obtained using the PSO optimization method as follows: $K_p = 14.5387 Nms/rad$, $K_i = 274.9991 Nm/rad$, and $\lambda = 0.8955$.

$$G_{PSO/FOPI}(s) = 14.5387 + \frac{274.999}{s^{0.8955}} \tag{27}$$

Therefore, the Oustaloup approach with $N = 5$, $\omega_b = 0.001 rad/s$ and $\omega_h = 1000 rad/s$ results in the following loop transfer function for the FOPI controller used as the speed regulator:

$$G_{\mathrm{PSO/FOPI}}(s) = \frac{\begin{array}{l}15.1s^5 + 1654s^4 + 3.39\times10^4 s^3 + \\ 1.003\times10^5 s^2 + 2.142\times10^4 s + \\ 275\end{array}}{\begin{array}{l}s^5 + 77.8s^4 + 3.599\times10^5 s^3 + \\ 1.043\times10^6 s^2 + 1.902\times10^4 s + \\ 0.002058\end{array}} \tag{28}$$

Figures 5 and 8 show the steady-state simulation results of the conventional DTC and the proposed DTC of DSIM.

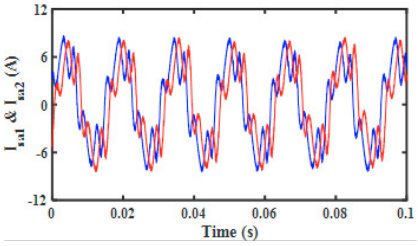

(a) Phase currents

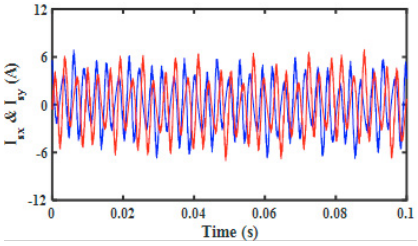

(b) Currents in (x-y) subspace

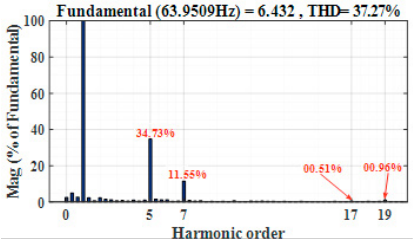

(c) THD

Fig. 5. Performance of Classical DTC.

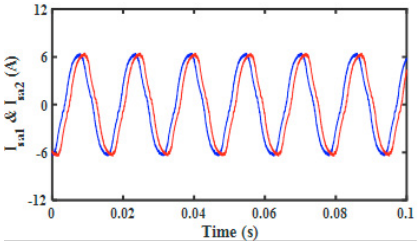

(a) Phase currents

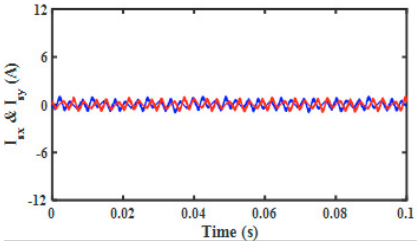

(b) Currents in (x-y) subspace

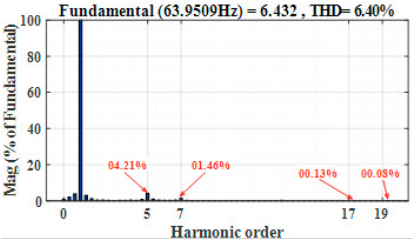

(c) THD

Fig. 6. Performance of Proposed DTC.

As shown in Fig. 5, the circulating current in subspace $(x-y)$ is clearly not controllable with conventional DTC, resulting in high harmonic currents. Figure 6 demonstrates the impact of integrating virtual voltage vectors into the switching table, which notably decreases the harmonic current components within the $(x-y)$ subspace. Figures 5 and 6 also show the total harmonic distortion (THD) of the phase current. It is evident that the proposed method reduces the 5th, 7th, 17th, and 19th order harmonics of the THD from 34.75%, 11.55%, 0.51%, and 0.96% to 4.21%, 1.46%, 0.13%, and 0.08%, respectively.

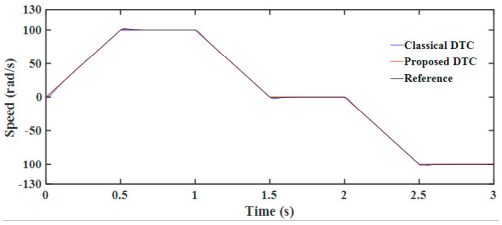

(a) Speed response

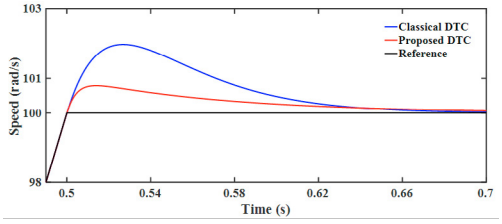

(b) Zoom

Fig. 7. Dynamic performance of Speed.

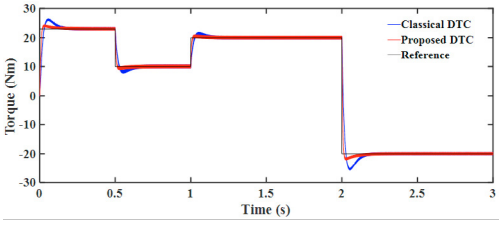

(a) Torque response

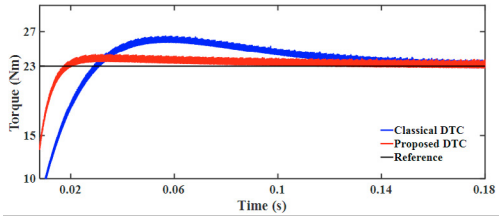

(b) Zoom

Fig. 8. Dynamic performance of Torque.

In order to analyze the speed reversal characteristics of the DSIM, simulations were performed using the following reference speed profiles: from 0 rad/s to 100 rad/s, from 100 rad/s to 0 rad/s, and from 0 rad/s to -100 rad/s, under a load of 10 Nm. As the machine speed increases from 0 to 100 rad/s and decreases from 100 rad/s to -100 rad/s, the speed response accurately tracks the reference in both control strategies, as illustrated in Figure 7. Under these conditions, the proposed FOPI controllers achieved the reference speed with a lower overshoot compared to the classical PI controller.

In addition, the proposed DTC shows a significant improvement in torque response, with lower overshoot and faster response time compared to the classical DTC. Furthermore, it is important to note that the critical parameters used for comparison, such as overshoot, settling time, and rise time, also support the use of the fractional-order controller in the DTC control of the DSIM (see Figure 8).

Table 2. Transient response comparison for various control methods (Speed = 100 rad/s, Torque = 10 Nm)

Different Techniques	Overshoot (%)	Settling Time (Sec)	Rise Time (Sec)
Classical DTC	1.9630	0.6468	0.4221
DTC method Guedida et al. (2024)	0.7064	0.5920	0.4205
Proposed DTC	0.7928	0.4916	0.3267

Table 2 shows a comparative study between the proposed technique, a recently published control strategy. It is worth mentioning that our approach exhibits dynamic performance similar to that of Guedida et al. (2024), with a better response compared to that of the classical DTC.

6. CONCLUSION

The classical DTC scheme for the DSIM suffers from significant harmonic currents. Moreover, the dynamic speed and torque performances obtained with conventional PI controllers can be improved. The main goal of this work is to eliminate components associated with harmonic subspace and obtain a better performance response of speed and torque. This work has been carried out by using 12 virtual voltage vectors and FOPI controllers based on the PSO algorithm with Oustaloup approximations. The simulation results indicate that the proposed DTC offers significantly enhanced dynamic performance, such as low overshoot and fast response, with a significant reduction in current harmonics compared to the classical DTC.

REFERENCES

E. Levi. Multiphase electric machines for variable-speed applications. *IEEE Transactions on Industrial Electronics*, 55(5):1893–1909, 2008.

M. J. Duran, I. Gonzalez-Prieto, N. Rios-Garcia and F. Barrero. A simple, fast, and robust open-phase fault detection technique for six-phase induction motor drives. *IEEE Transactions on Power Electronics*, 33(1): 547–557, 2017.

S. Guedida, B. Tabbache, K. Nounou, and M. Benbouzid. Direct torque control scheme for less harmonic currents and torque ripples for dual star induction motor. *Revue Roumaine des Sciences Techniques—Série Électrotechnique Et Énergétique*, 68(4):331–338, 2023.

G. Boukhalfa, S. Belkacem, A. Chikhi, and S. Benaggoune. Direct torque control of dual star induction motor using a fuzzy-PSO hybrid approach. *Applied Computing and Informatics*, 18(1/2):74–89, 2022.

S. Guedida, B. Tabbache, K. Nounou, and A. Idir. Reduced-Order Fractionalized Controller for Disturbance Compensation Based on Direct Torque Control of DSIM With Less Harmonic. *Electrica*, 24(2), 2024.

E. S. Terfia, S. E. Rezgui, S. Mendaci, H. Gasmi, and H. Benalla. Optimal Fractional Order Proportional Integral Controller for Dual Star Induction Motor Based on Particle Swarm Optimization Algorithm. *Journal Européen des Systèmes Automatisés*, 56(2), 2023.

R. Belal, M. Flitti, and M. L. ZEGAI. Tuning of PI Speed Controller in Direct Torque Control of Dual Star Induction Motor Based on Genetic Algorithms and Neuro-Fuzzy Schemes. *Revue roumaine des Sciences Techniques—Série Électrotechnique et Énergétique*, 69(1), 9–14, 2024.

A. Idir, H. Akroum, M. Nesri, S. Guedida and L. Canale. Design and Performance Evaluation of a Novel FOPID Control Strategy for Electric Furnace Temperature Regulation using HHO Algorithm. *Applications of Modelling and Simulation*, 9:349–362, 2025.

I. Podlubny, L. Dorcak, and I. Kostial. On fractional derivatives, fractional-order dynamic system and PID-controllers. In *Proceedings of the 36th IEEE Conference on Decision and Control*, pages 4985–5990, December 1999.

V. S. R. Chagam and S. Devabhaktuni. Enhanced low-speed characteristics with constant switching torque-controller-based DTC technique of five-phase induction motor drive with FOPI control. *IEEE Transactions on Industrial Electronics*, 70(11):10789–10799, 2022.

J. J. Di Gud, Teodoro, A., Camacho, O. and Bringas, P. G. A new fractional reduced-order model-inspired system identification method for dynamical systems. *IEEE Access*, (11):103214–103231, 2023.

Zhao, Y., and Lipo, T. A. Space vector PWM control of dual three-phase induction machine using vector space decomposition. *IEEE Transactions on industry applications*, 31(5):1100–1109, 1995.

Sifelislam, G., Bekheira, T., Kamal, N., Mokhtar, N., and Idir, A. Virtual vector-based neural network DTC scheme for dynamic performance improvement of dual-star induction motor drive. *e-Prime-Advances in Electrical Engineering, Electronics and Energy*, 11:100938, 2025.

Ren, Y., and Zhu, Z. Q. Enhancement of steady-state performance in direct-torque-controlled dual three-phase permanent-magnet synchronous machine drives with modified switching table. *IEEE Transactions on Industrial Electronics*, 62(6):3338–3350, 2014.

Sabatier, J., Oustaloup, A., Iturricha, A. G., and Levron, F. CRONE control of continuous linear time periodic systems: Application to a testing bench. *ISA transactions*, 42(3):421–436, 2003.

Garrappa, R. A Grunwald–Letnikov scheme for fractional operators of Havriliak–Negami type. *Recent Advances in Applied, Modelling and Simulation*, 34:70–76, 2014.

Oustaloup, A., Levron, F., Mathieu, B., and Nanot, F. M. Frequency-band complex noninteger differentiator: characterization and synthesis. *IEEE Transactions on Circuits and Systems I: Fundamental Theory and Applications*, 47(1):25–39, 2000.

Nesri, M., Nounou, K., Marouani, K., Houari, A., and Benkhoris, M. F. Efficiency improvement of a vector-controlled dual star induction machine drive system. *Electrical Engineering*, 102(2):939–952, 2020.